Bioorganic & Medicinal Chemistry Letters xxx (2017) xxx–xxx

Contents lists available at ScienceDirect

Bioorganic & Medicinal Chemistry Letters

journal homepage: www.elsevier.com/locate/bmcl

Synthesis and evaluation of ^{11}C-labeled coumarin analog as an imaging probe for detecting monocarboxylate transporters expression

Hiroyuki Tateishi [a,e], Atsushi B. Tsuji [a,*], Koichi Kato [b,c,*], Hitomi Sudo [a], Aya Sugyo [a], Takashi Hanakawa [c], Ming-Rong Zhang [b], Tsuneo Saga [a,d], Yasushi Arano [e], Tatsuya Higashi [a]

[a] Experimental Nuclear Medicine Team, Department of Molecular Imaging and Theranostics, National Institute of Radiological Sciences, National Institutes for Quantum and Radiological Science and Technology (QST-NIRS), 4-9-1 Anagawa, Inage-ku, Chiba 263-8555, Japan
[b] Department of Radiopharmaceuticals Development, National Institute of Radiological Sciences, National Institutes for Quantum and Radiological Science and Technology (QST-NIRS), 4-9-1 Anagawa, Inage-ku, Chiba 263-8555, Japan
[c] Department of Integrative Brain Imaging, National Center of Neurology and Psychiatry, 4-1-1 Ogawahigashi-cho, Kodaira, Tokyo 187-5551, Japan
[d] Department of Diagnostic Radiology, Kyoto University Hospital, 54 Shogoinkawahara-cho, Sakyo-ku, Kyoto 606-8507, Japan
[e] Department of Molecular Imaging and Radiotherapy, Graduate School of Pharmaceutical Sciences, Chiba University, 1-8-1 Inohana, Chuo-ku, Chiba 260-8675, Japan

ARTICLE INFO

Article history:
Received 30 June 2017
Revised 11 September 2017
Accepted 14 September 2017
Available online xxxx

Keywords:
Positron emission tomography
Fluorescence
Cancer
Astrocyte–neuron lactate shuttle
Radiosynthesis

ABSTRACT

Upregulated monocarboxylate transporters (MCTs) in tumors are considered diagnostic imaging targets. Herein, we synthesized the positron emission tomography probe candidates coumarin analogs **2** and **3**, and showed 55 times higher affinity of **2** for MCTs than a representative MCT inhibitor. Whereas **[^{11}C]2** showed low tumor accumulation, probably due to adduct formation with plasma proteins, **[^{11}C]2** showed high initial brain uptake, suggesting that the scaffold of **2** has properties that are preferable in imaging probes for the astrocyte–neuron lactate shuttle. Although further optimization of **2** is required, our findings can be used to inform the development of MCT-targeted imaging agents.

Monocarboxylate transporters (MCTs) belong to the SLC16 gene family, which comprises 14 members. Among these, MCT1, MCT2, MCT3, and MCT4 are proton symporters that mediate bidirectional transmembrane transport of short chain monocarboxylates such as pyruvate, lactate and ketone bodies. Most living cells consume these monocarboxylates as fuel for the tricarboxylic-acid cycle,[1,2] indicating that MCTs play important roles in cell homeostasis.

In many tumors, MCT1 and MCT4 highly express and mediate lactate transport.[3] Lactate is produced from aggressive tumor metabolism such as glycolysis,[4,5] glutaminolysis,[6–8] and serinolysis,[6] and acidifies tumor microenvironments, promoting tumor malignancy and invasiveness, and leading to poor clinical outcomes.[9–14] Recently, lactate has been recognized as a key energy source for tumor metabolic symbiosis, in which oxidative tumor cells consume lactate from glycolytic cells.[15–17] Thus, lactate is not merely a waste metabolite but also a key intermediate for tumor metabolism. Consequently, aberrant lactate metabolism is considered a hallmark of cancer and the lactate transporters MCT1 and MCT4 are attractive targets for cancer diagnosis and therapy. Hence, radiolabeled inhibitors of MCT1 and/or MCT4 with positron emitting radionuclides such as ^{11}C and ^{18}F have potential as imaging agents for cancer diagnoses using positron emission tomography (PET), which is a non-invasive quantitative imaging technique with high sensitivity that can be used to monitor pathophysiological changes and disease progression.[18]

Although α-cyano-4-hydroxycinamic acid (CHC) is a well-known MCT inhibitor (Fig. 1), it has low affinity (11 μM) and specificity for MCTs.[19–21] Recently, Draoui et al. synthesized several 3-carboxy-coumarin derivatives and evaluated their inhibitory activities against MCTs.[21] These investigators reported that 7-alkylamino substituents on 3-carboxy-coumarin scaffolds were required for significant inhibition of MCTs.[21] Among presented compounds, that with a 7-benzyl(methyl)amino substituent **1** (Fig. 1) showed the strongest inhibition of lactate influx (IC_{50}, 11 nM) and the corresponding ^{11}C-labeled compound [*N*-^{11}C-methyl]**1** was considered a candidate PET probe. However, a distinct synthesis scheme is required for a dimethyl precursor for

* Corresponding authors at: Department of Molecular Imaging and Theranostics, National Institute of Radiological Sciences, National Institutes for Quantum and Radiological Science and Technology (QST-NIRS), 4-9-1 Anagawa, Inage-ku, Chiba 263-8555, Japan (A.B. Tsuji); Department of Integrative Brain Imaging, National Center of Neurology and Psychiatry, 4-1-1 Ogawahigashi-cho, Kodaira, Tokyo 187-5551, Japan (K. Kato).

E-mail addresses: tsuji.atsushi@qst.go.jp (A.B. Tsuji), katok@ncnp.go.jp (K. Kato).

https://doi.org/10.1016/j.bmcl.2017.09.033
0960-894X/

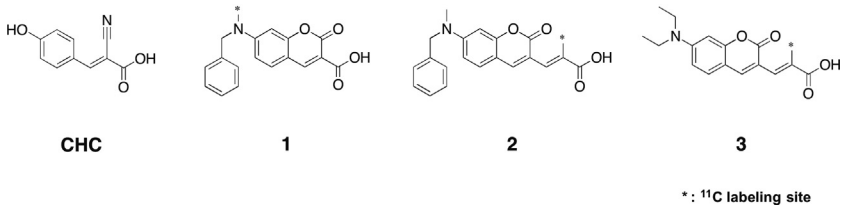

Fig. 1. Structure of α-cyano-4-hydroxycinamic acid (CHC) and monocarboxylate transporter (MCT)-targeting candidates **1**, **2**, and **3**. *Represents the ^{11}C-labeling site.

^{11}C labeling of **1** that is directed our attention to more accessible targets. Thus, we considered the use of another benzyl(methyl) amino analog **2** (Fig. 1) for the development of an MCT-targeted imaging probe, because both **2** and the appropriate non-radioactive precursor to synthesize ^{11}C-labeled **2** (**[^{11}C]2**) can be prepared via the common aldehyde intermediate **7**. In addition, both the diethylamino analog **3** (Fig. 1) and the appropriate non-radioactive precursor **11** could be prepared using a similar synthetic scheme.[22] Furthermore, ^{11}C-labeled **2** and **3** can be synthesized by our labeling method to construct versatile ^{11}C-labeled olefin frameworks based on Horner-Wadsworth-Emmons (HWE) reactions.[22] In the present study, we synthesized the benzyl(methyl)amino analog **2** and the diethylamino analog **3** and performed *in vitro* studies using human cancer cell lines. We also demonstrated ^{11}C-labeling synthesis of **2** and evaluated temporal radioactivity change of **[^{11}C]2** in a tumor mouse model by dynamic PET study.

Compounds **2** and **3** were synthesized as shown in Schemes 1 and 2, respectively, according to previous reports.[21,22] During the synthesis of **2**, Knoevenagel condensation of 7-amino substituted salicylaldehyde **5** with Merdrum's acid was used to construct the 3-carboxy-coumarin skeleton **1**. Salicylaldehyde **5** was obtained from two steps, involving Buchwald–Hartwig cross coupling of 3-bromophenol with *N*-methyl-1-phenylmethanamine, followed by a Vilsmeier–Haack reaction. The carboxyl group of **1** was then converted to the corresponding aldehyde **7**. The subsequent HWE reaction afforded **8** and **2** was obtained after hydrolysis of the ethyl ester. Subsequently, **3** was synthesized according to a similar scheme (Scheme 2). Overall, a yield of 23.3% was achieved from the 7-step synthesis for **2** and a yield of 45.1% was achieved from the 5-step synthesis for **3**. The *E*/*Z* isomeric mixture of **2** and **3** was used for *in vitro* and *in vivo* studies due to their ease of photo-isomerization (Supplementary Fig. 1). Compounds **2** and **3** showed strong blue–green fluorescence (Table 1).

Lactate uptake inhibition assays of **2** and **3** were conducted using [^{14}C]lactate and Becker tumor cells. As shown in Fig. 2, compounds **2** and **3** dose-dependently inhibited lactate uptake with IC_{50} values of 0.2 μM for **2**, 9.3 μM for **3**, and 11 μM for CHC. The IC_{50} value for **2** was approximately 55 times greater than that for CHC, which was similar to that of **3**. We therefore chose to use **2** in further studies.

Expression analyses of MCT1 and MCT4 were performed using quantitative RT-PCR in Becker, AsPC-1 and MDA-MB-231 human cancer cell lines. These experiments showed that Becker cells express MCT1 at the highest levels, followed by AsPC-1 and MDA-MB-231 cells (Fig. 3 left panel). MCT4 expression was greatest in MDA-MB-231 cells, followed by Becker and AsPC-1 cells (Fig. 3 right panel).

As shown in Fig. 4, Becker cells showed the highest uptake of **2**, followed by AsPC-1 and MDA-MB-231 cells. Taken together, these data suggest that **2** was transported into cells in an MCT1-expression-dependent manner, likely reflecting differences in the MCT1 and MCT4 binding affinity of monocarboxylates such as **2**. Accordingly, compared with MCT1, the affinity of MCT4 for monocarboxylates was lower, and the affinity of MCT4 for L-lactate (Km, 28.0–34.0 mM) was also lower than that of MCT1 (Km, 2.2–4.5 mM).[3]

As shown in Scheme 3, **[^{11}C]2** was synthesized using a 3-step synthesis protocol. Both ^{11}C-methylation of phosphonate and subsequent HWE reaction of the aldehyde precursor **7** with the ^{11}C-methylated phosphonate were performed in the presence of tetrabutylammonium fluoride as a base, and subsequent alkaline hydrolysis of the ethyl ester afforded **[^{11}C]2**.[22] Analytical HPLC chromatograms of each step were shown in Supplementary Fig. 2. The radiosynthesis time of **[^{11}C]2** was approximately 50 min and radiochemical yields were 6.6% and 5.2% (n = 2, decay-uncorrected). The radiochemical purity was over 95% and *E*/*Z* ratio was approximately 9:1 (Supplementary Fig. 2).

To evaluate the pharmacokinetics of **[^{11}C]2** *in vivo*, 11.8 MBq of **[^{11}C]2** was intravenously administered to a mouse bearing Becker tumor xenograft and dynamic PET study was conducted. Temporal PET images and time activity curves of interested organs are presented in Fig. 5. The radiotracer **[^{11}C]2** was rapidly cleared from the blood and was excreted through the kidneys and hepatobiliary tract (Fig. 5A and B). High liver uptake of **[^{11}C]2** was observed, with a peak value of 16.0% ID/g at 270 s, and radioactivity decreased thereafter to 6.5% ID/g at 3300 s (Fig. 5C). Contrary to expectations, tumor accumulation of **[^{11}C]2** was low with a peak value of only

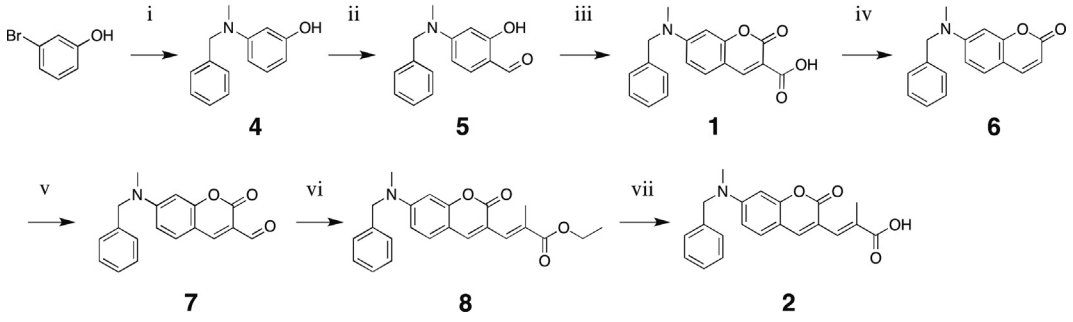

Scheme 1. Synthesis of compound **2**. Reagents and conditions: (i) *N*-methyl-1-phenylmethanamine, $Pd_2(dba)_3$, (2-biphenyl)di-*tert*-butylphosphine, LHMDS in THF, reflux for 16 h; (ii) $POCl_3$ in DMF, 0–60 °C for 7 h; (iii) Meldrum's acid, piperidine, AcOH in EtOH, 90 °C for 8 h; (iv) 18% HCl aq., reflux for 6 h; (v) $POCl_3$ in DMF, 0–60 °C for 7 h. (vi) triethylphosphonopropionate, NaH in THF, 90 °C for 6 h; (vii) 2 M NaOH in MeCN, rt for 12 h.

Please cite this article in press as: Tateishi H., et al. Bioorg. Med. Chem. Lett. (2017), https://doi.org/10.1016/j.bmcl.2017.09.033

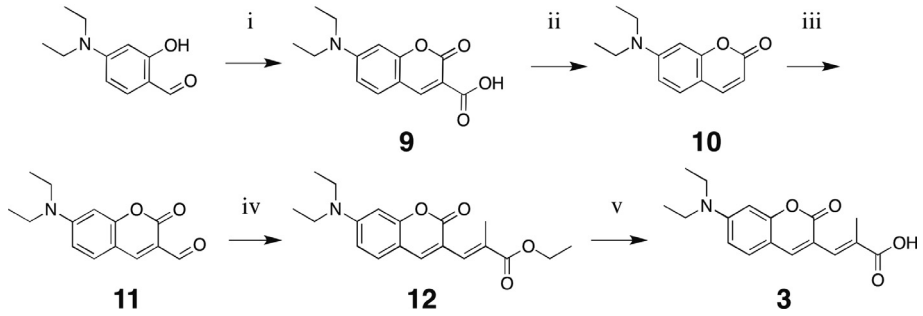

Scheme 2. Synthesis of compound **3**. Reagents and conditions: (i) Meldrum's acid, piperidine, AcOH in EtOH, 90 °C for 6 h; (ii) 18% HCl aq., reflux for 6 h; (iii) $POCl_3$ in DMF, 0–60 °C for 7 h; (iv) triethylphosphonopropionate, NaH in THF, 90 °C for 6 h; (v) 2 M NaOH in MeCN, rt for 12 h.

Table 1
Fluorescence properties of compound **2** and **3**.

Compound	CHC	2	3
Excitation/Emission	No fluorescence	395/504	410/508
Fluorescence quantum yield (ϕ)	–	0.16	0.15

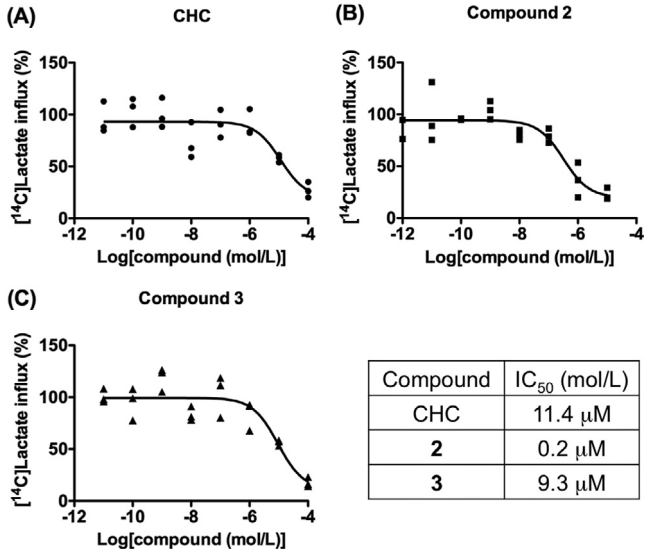

Compound	IC_{50} (mol/L)
CHC	11.4 μM
2	0.2 μM
3	9.3 μM

Fig. 2. Competitive inhibition assays of lactate influx withα-cyano-4-hydroxycinnamic acid (CHC) (A), compounds **2** (B) and compound **3** (C). [^{14}C]lactate uptake in Becker cells was determined by measuring intracellular radioactivity after 60-min incubation with each inhibitor (n = 3) at 37 °C. Radioactivity was normalized by protein amount. IC_{50} is the compound concentration (mol/L) that reduces lactate uptake by 50%.

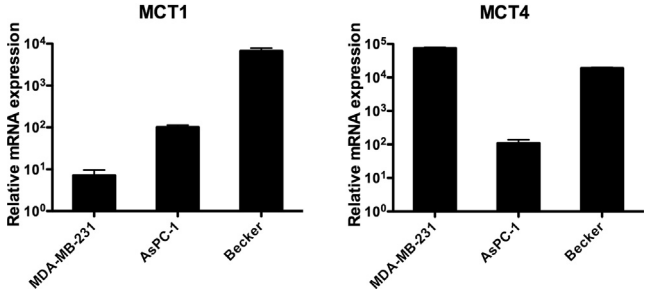

Fig. 3. Expression of MCT1 and MCT4 mRNA in three cell lines. Relative mRNA expression levels of MCT1 and MCT4 in Becker, AsPC-1, and MDA-MB-231 cells (n = 3); mRNA expression levels in AsPC-1 cells were taken as 100. Fold changes in expression were determined using the ΔΔCt method and were normalized to those of the 18S rRNA internal control.

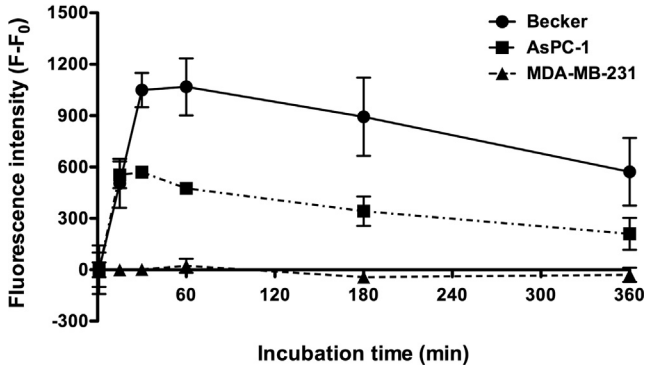

Fig. 4. Cell uptake of **2** in three cell lines. Uptake of **2** into Becker, AsPC-1, and MDA-MB-231 cells (n = 3); cells were incubated with 10^{-5} M of **2** in 1 mL of PBS for 1, 15, 30, 60, 180 and 360 min. Uptake of **2** into cells was then measured according to fluorescence intensities with excitation at 395 nm and emission at 504 nm. Fluorescence intensities were normalized to protein contents, which were determined using Bradford protein quantification methods. At the vertical axis, "$F–F_0$" represents "(fluorescence intensity at each time point)–(fluorescence intensity at 0 min)."

1.9% ID/g at 210 s (Fig. 5D). According to metabolite analysis (Supplementary Fig. 3), approximately 27% of radioactivity were observed as radiometabolites. Although PET images using **[^{11}C]2** mainly reflect the intact form, we need to consider radiometabolites for more precise implication in further study.

To determine why **[^{11}C]2** accumulation was low in tumor, we then performed plasma protein binding test and demonstrated a plasma protein binding rate of 92.0% ± 4.1% (n = 3) after 30-min incubation with mouse plasma, indicating almost complete binding of **[^{11}C]2** to plasma proteins. This high protein binding may reflect reversible binding as well as Michael addition reaction of thiols of plasma protein[23,24] since **[^{11}C]2** contains electron deficient olefin. Most of **[^{11}C]2** would bind to plasma proteins and the remaining **[^{11}C]2** would accumulate highly in the liver, which is considered to be the cause of low tumor uptake of **[^{11}C]2**.

In contrast with the low tumor accumulation, **[^{11}C]2** was readily taken up into brain region and uptake of radioactivity after injections peaked at 7.6% ID/g at 35 s post administration, although the high radioactivity in the brain region, **[^{11}C]2** disappeared quickly (Fig. 5E). Because MCT1 expresses at blood-brain barrier and cerebral blood flow is greater than tumor blood flow, **[^{11}C]2** may be transported into the brain before conjugation with plasma proteins. We therefore considered the molecular properties of the scaffold of **2** as preferable for passage through the blood-brain barrier. However, insufficient affinity of **[^{11}C]2** for MCT1 may cause low retention, resulting in rapid clearance from the brain. Brain MCT1 is predominantly expressed in astrocytes and is involved in the astrocyte–neuron lactate shuttle (ANLS).[25,26] The ANLS plays

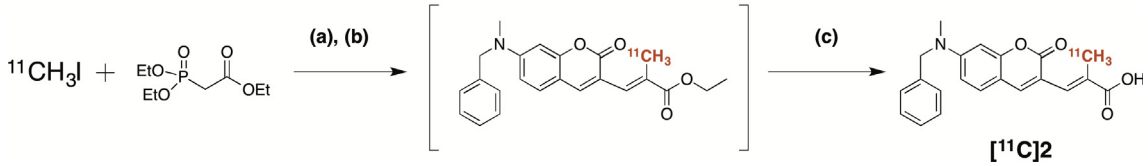

Scheme 3. Synthetic of **[^{11}C]2**. Reagents and conditions: (a) TBAF, THF, 30 °C, 3 min; (b) compound **7**, 70 °C, 7 min; (c) 2 M NaOH aq., 25 °C, 8 min.

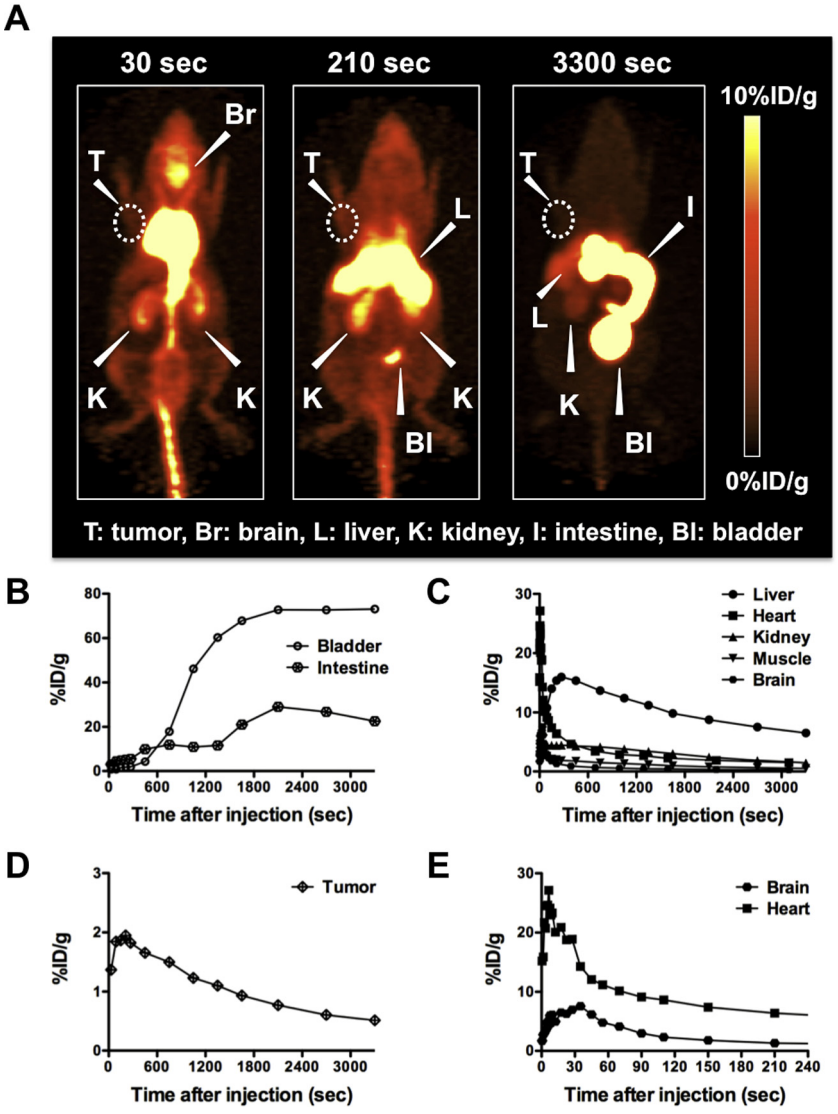

Fig. 5. PET images and time activity curves (TAC) in organs of interest. A, PET images (maximum intensity projection) at 30, 210, and 3300 s after administration of **[^{11}C]2**; B, TAC of bladder and intestine; C, TACs of liver, heart, kidney and muscle; D, TAC of Becker tumors; E, Expanded widow of TAC of brain and heart.

important roles in energy metabolism and survival of neurons like tumor cells, and decreased activity of ANLS is considered a hallmark of neurodegenerative disease.[27] In addition, several studies indicate that lactate acts as a key neuroprotective substance to CNS disorders.[28–30] Therefore, MCT1-targeted imaging may facilitate further studies of pathological mechanisms of CNS disorders. Thus, further improvements of the inhibitory ability of **2** against MCT1 will follow structure optimization of the scaffold of **2** by changing the 7-amino substituent, which significantly impacts affinity for MCTs.[21]

In conclusion, 7-amino carboxycoumarin derivatives **2** and **3** were synthesized, and **2** had approximately 55 times higher affinity for MCTs than the representative MCT inhibitor CHC. Compound **2** was also transported into cells predominantly by MCT1. Although **2** was radiolabeled with ^{11}C using our labeling method, the high protein binding affinity prevented uptake of **[^{11}C]2** into tumors. However, we observed high initial **[^{11}C]2** uptake into the brain and subsequent rapid clearance. The present data warrant further development of MCT-targeted PET imaging agents based on 7-amino-3-carboxy-coumarin.

Please cite this article in press as: Tateishi H., et al. Bioorg. Med. Chem. Lett. (2017), https://doi.org/10.1016/j.bmcl.2017.09.033

Acknowledgments

We thank Naoko Kuroda and Yuriko Ogawa for technical assistance, Nobuki Nengaki and Hisashi Suzuki for producing the radioisotope and providing technical support for remote-controlled synthesis, the staff of the Cyclotron Operation section for cyclotron operation, and Tomoya Uehara and Hiroyuki Suzuki for MS operation. This work was supported in part by KAKENHI 15K09976, 15K19831, and 16K10304.

A. Supplementary data

Supplementary data associated with this article can be found, in the online version, at http://dx.doi.org/10.1016/j.bmcl.2017.09.033.

References

1. Pérez-Escuredo J, Van Hée VF, Sboarina M, et al. *Biochim Biophys Acta*. 2016;1863:2481.
2. Halestrap AP, Price NT. *Biochem J*. 1999;343:281.
3. Pinheiro C, Longatto-Filho A, Azevedo-Silva J, Casal M, Schmitt FC, Baltazar F. *J Bioenergy Biomembr*. 2012;44:127.
4. Vander Heiden MG, Cantley LC, Thompson CB. *Science*. 2009;324:1029.
5. Lu H, Forbes RA, Verma A. *J Biol Chem*. 2002;277:23111.
6. Mazurek S, Drexler HCA, Troppmair J, Eigenbrodt E, Rapp UR. *Anticancer Res*. 2007;27:3963.
7. DeBerardinis RJ, Mancuso A, Daikhin E, et al. *Proc Natl Acad Sci USA*. 2007;104:19345.
8. Mazurek S, Zwerschke W, Jansen-Durr P, Eigenbrodt E. *Biochem J*. 2001;356:247.
9. Schwickert G, Walenta S, Sundfor K, Rofstad EK, Mueller-Klieser W. *Cancer Res*. 1995;55:4757.
10. Spector JA, Mehrara BJ, Greenwald JA, et al. *Am J Physiol Cell Physiol*. 2001;280:C72.
11. Dhup S, Dadhich RK, Porporato PE, Sonveaux P. *Curr Pharm Des*. 2012;18:1319.
12. Walenta S, Salameh A, Lyng H, et al. *Am J Pathol*. 1997;150:409.
13. Walenta S, Wetterling M, Lehrke M, et al. *Cancer Res*. 2000;60:916.
14. Kumar VBS, Viji RI, Kiran MS, Sudhakaran PR. *J Cell Physiol*. 2007;211:477.
15. Hirschhaeuser F, Sattler UG, Mueller-Klieser W. *Cancer Res*. 2011;71:6921.
16. Sonveaux P, Vegran F, Schroeder T, et al. *J Clin Invest*. 2008;118:3930.
17. Vegran F, Boidot R, Michiels C, Sonveaux P, Feron O. *Cancer Res*. 2011;71:2550.
18. Vaquero JJ, Kinahan P. *Annu Rev Biomed Eng*. 2015;17:385.
19. Hildyard JCW, Halestrap AP. *Biochem J*. 2003;374:607.
20. Wang X, Levi AJ, Halestrap AP. *Am J Physiol*. 1996;270:476.
21. Draoui N, Schicke O, Fernandes A, et al. *Bioorg Med Chem*. 2013;21:7107.
22. Takashima M, Kato K, Ogawa M, Magata Y. *RSC Adv*. 2013;3:21275.
23. Kwon H, Lee K, Kim HJ. *Chem Commun (Camb)*. 2011;47:1773.
24. Sun YQ, Chen M, Liu J, Lv X, Li JF, Guo W. *Chem Commun (Camb)*. 2011;47:11029.
25. Pellerin L, Magistretti PJ. *Proc Natl Acad Sci USA*. 1994;91:10625.
26. Rouach N, Koulakoff A, Abudara V, Willecke K, Giaume C. *Science*. 2008;322:1551.
27. Newington JT, Harris RA, Cumming RC. *J Neurodegener Dis*. 2013;2013:234572.
28. Cureton EL, Kwan RO, Dozier KC, Sadjadi J, Pal JD, Victorino GP. *J Surg Res*. 2010;159:468.
29. Coco M, Caggia S, Musumeci G, et al. *J Neurosci Res*. 2013;91:313.
30. Voss MW, Erickson KI, Prakash RS, et al. *Brain Behav Immun*. 2013;28:90.